Nanoscale

PAPER

View Article Online
View Journal | View Issue

Cite this: *Nanoscale*, 2020, **12**, 6821

Platinum nanoparticles stabilized by N-heterocyclic thiones. Synthesis and catalytic activity in mono- and di-hydroboration of alkynes†

Leonardo C. Moraes,[a,b] Rute C. Figueiredo,[a,c] Juan P. Espinós,[d] Florencia Vattier,[d] Antonio Franconetti,[e] Carlos Jaime,[e] Bertrand Lacroix,[f,g] Javier Rojo,[a] Patricia Lara*[a,b] and Salvador Conejero*[a,b]

N-Heterocyclic Thiones (NHT) proved to be efficient ligands for the stabilization of small platinum nanoparticles (1.3–1.7 nm), synthesized by decomposition of $[Pt(dba)_2]$, under a H_2 atmosphere, in the presence of variable sub-stoichiometric amounts of the NHT. Full characterization by means of TEM, HR-TEM, NMR, ICP, TGA and XPS have been carried out, providing information about the nature of the metal nanoparticles and the interaction of the NHT ligands to the metal surface. Importantly, DFT calculations indicate that some NHT ligands interact with the metal through the C=C double bond of the imidazole fragment in addition to the sulfur atom, thus providing additional stabilization to the nanoparticles. According to XPS, TGA and ICP techniques, the surface coverage by the ligand increases by decreasing the size of the substituents on the nitrogen atom. The platinum nanoparticles have been used as catalyst in the hydroboration of alkynes. The most active system is that with a less covered surface area lacking an interaction of the ligand by means of the C=C double bond. This catalyst hydroborates alkynes with excellent selectivities towards the monoborylated anti-Markovnikov product (vinyl-boronate) when one equiv. of borane is used. Very interestingly, aliphatic alkynes undergo a second hydroborylation process leading to the corresponding 1,1- and 1,2-diboroylated species with good selectivities towards the former.

Received 9th January 2020,
Accepted 8th March 2020

DOI: 10.1039/d0nr00251h

rsc.li/nanoscale

Introduction

Metal nanoparticles (NPs) are nowadays well recognized materials with potential applications in different research areas spanning from electronic devices to catalysis.[1] Most specifically, platinum nanoparticles have played a major role in important catalytic processes such as the oxygen reduction reaction,[2] oxidation of CO[3] or hydrosilylation[4] to name a few. The small size of the metal nanoparticles improves its chemical reactivity or even their selectivity.[5] The shape, size and ligand coating of the NPs dictate its catalytic behavior and thus most of the research groups have focused their attention on these parameters to control the activity and selectivity of the processes.[6] With respect to the stabilizer of the metal nanoparticle, most of the ligands used for unsupported platinum systems are based on thiols,[7] phosphines[8] and amines,[9] ligands that bind the metal strongly enough to prevent agglomeration processes. This is in stark contrast to the acquired knowledge that we have in molecular chemistry, for which a vast library of ligands have been used over the years to tune the properties of their corresponding platinum complexes. In recent years, some efforts have been made to transfer this knowledge to the realm of the metal nanoparticles, with some relevant illustrative examples in the use of the now prevalent N-heterocyclic carbenes (still under-developed in the field of metal nanoparticles),[10] zwitterionic amidinates[11] or other type of reactive (non-innocent) carbenes and vinyli-

[a]*Instituto de Investigaciones Químicas (IIQ), CSIC – Universidad de Sevilla, C/ Américo Vespucio 49, 41092 Seville, Spain. E-mail: sconejero@iiq.csic.es, patricia@iiq.csic.es*
[b]*CSIC and Universidad de Sevilla, Departamento de Química Inorgánica, Centro de Innovación en Química Avanzada (ORFEO-CINQA), Spain*
[c]*Universidade Federal de Ouro Preto, Departamento de Química, Instituto de Ciências Exatas e Biológicas, Rua Costa Sena, 171, Centro, 35400-000, Ouro Preto, Minas Gerais, Brazil*
[d]*Nanotechnology on Surfaces Laboratory, Instituto de Ciencia de Materiales de Sevilla (ICMS), CSIC – Universidad de Sevilla, c/Américo Vespucio 49, 41092 Sevilla, Spain*
[e]*Departament de Química, Universitat Autònoma de Barcelona, 08193 Cerdanyola del Vallès, Spain*
[f]*Department of Materials Science and Metallurgical Engineering, and Inorganic Chemistry, University of Cádiz, Spain*
[g]*IMEYMAT, Institute of Research on Electron Microscopy and Materials of the University of Cádiz, Spain*

†Electronic supplementary information (ESI) available: Synthesis and characterization of PtNP-NHTs. Catalytic procedures. Spectroscopic data of boron compounds. Computational methods. See DOI: 10.1039/d0nr00251h

denes.[12] These ligands modify the properties of the surface of the metal nanoparticle both electronically and sterically, and thus open the door for controlling their stability and catalytic performance. Very recently, we have succeeded in introducing N-heterocyclic thiones (NHTs) as ligand stabilizers for gold NPs.[13] This success was due, in part, to the presence of a sulfur atom on the ligand that, beside forming a strong interaction with the gold surface, can adopt a resonant form with a negative charge on it that confers good coordinating properties to the NHT and a thiolate-like behavior (Fig. 1). In addition, some of the advantages of these types of ligands are found on the simplicity of their synthesis, the easiness of tuning their steric environment and their tolerance to air and protic solvents, which facilitates considerably their handling or their use during the synthesis of the metal NPs.[13] Platinum has also an excellent affinity to sulfur based ligands,[7c–e] with the paradigmatic example on the thiolate based platinum nanoparticles,[7] for which extensive utilization has been reported. Therefore, we have considered that NHTs could also be excellent ligand stabilizers for platinum nanoparticles. Moreover, non-supported platinum nanoparticles have been barely used in hydroboration reaction of alkynes,[10c,14] a process that lead to the formation of C–B bonds, which are starting materials for a myriad of organic transformations.[15] There have been some reports on the use of metal nanoparticles for the hydroboration of alkynes. However, the boron source for such transformations are based on diboron reagents, which usually requires the use of external additives and have the inconvenient of losing half of the boron source, and consequently the generation of large amounts of waste.[16] In this sense, the search for catalytic systems that can incorporate into an unsaturated organic fragment (alkynes) two boryl units through diborylation reactions is gaining relevance, since such organoboron compounds can be further poly-functionalized. Moreover, diborylation processes have been considerably less explored, although some important contributions have recently appeared in the literature by using homogeneous catalysts.[17] The large surface area found in metal (platinum) nanoparticles might be relevant to achieve a sufficient active catalyst able to diborylate alkynes.

In this contribution, we wish to report the synthesis of well-defined, small platinum nanoparticles stabilized by N-heterocyclic thiones, their characterization by different methods (including TEM, HR-TEM, XPS, NMR, ICP and TGA) and their use for the hydroboration of alkynes with hydroboranes. Additionally, DFT calculations have provided some clues about the coordination mode of the NHT to the surface of the NPs. We have found that some of these platinum nanoparticles are very efficient in the hydroboration of alkynes, leading to either mono- or diborylated species.

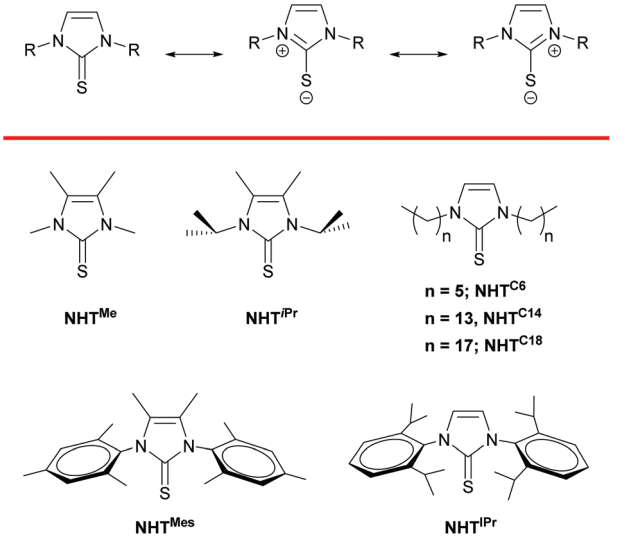

Fig. 1 Top: Resonant structure of N-heterocyclic thiones (NHTs). Bottom: N-Heterocyclic thiones used in this work.

Results and discussion

Synthesis and characterization of platinum-NHT nanoparticles

We have considered the use of different types of N-heterocyclic thiones with different substituents on the nitrogen atom, either aromatic or alkylic, the latter with different lengths to improve the stability of the platinum nanoparticle (see Fig. 1). We have used the organometallic method developed by Chaudret *et al.* for the synthesis of the metal nanoparticles,[18] using as starting material the Pt(0) complex bis(dibenzylideneacetone)platinum, [Pt(dba)$_2$], in the presence of variable amounts of the NHT ligands under a H_2 atmosphere (see ESI;† Scheme 1). Employing this methodology, we can get well-controlled metallic nanostructures in terms of shape, size dispersion, organization and surface state. The amount of ligand employed as stabilizer plays a key role in the characteristics of the nanostructures. Particularly, in the organometallic approach, a bottom-up method, individual Pt nuclei are present in the reaction media. In order to avoid the formation of traditional organometallic complexes, sub stoichiometric amounts of stabilizing ligands (typically between 0.2 to 0.5 equiv.) must be employed (see below). Purification of the Pt NPs can be easily achieved through successive washing with pentane at low temperature (see ESI† for details). Under these reaction conditions, well defined platinum NPs can be obtained depending on the structure and the amount of the NHT present during decomposition of the platinum starting material. Thus, methyl substituents at the nitrogen atom of

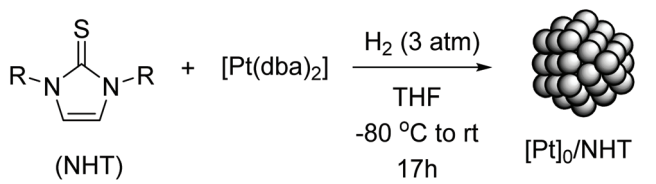

Scheme 1 Reaction conditions for the synthesis of the platinum nanoparticles.

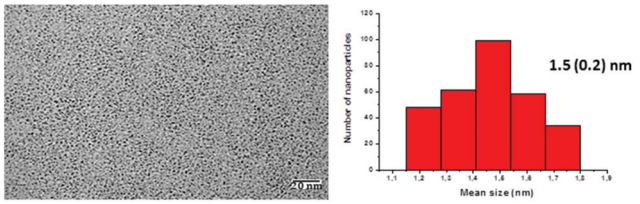

Fig. 2 TEM image of platinum nanoparticles PtNP-NHT^{iPr} synthesized from $Pt(dba)_2$ and 0.5 equiv. of NHT^{iPr}.

the NHT (NHT^{Me}) don't seem to be sufficiently bulky to form stable Pt NPs, neither using 0.2 nor 0.5 equiv. of this ligand per [$Pt(dba)_2$]. However, increasing the steric bulk by changing the methyl groups by iso-propyl fragments has a great impact on the formation of well-defined platinum NPs. Nevertheless, the amount of ligand present during decomposition of the platinum metal complex is very important to avoid the formation of agglomerates. Thus, 0.5 equiv. of NHT^{iPr} are at least needed to produce Pt NPs of mean-size 1.5(0.2) nm (Fig. 2) with a narrow distribution, whereas 0.2 equiv. lead to large amounts of agglomerates according to TEM images (see ESI, Fig. S16†). Similar behavior has been observed for ligands NHT^{C6}, NHT^{C14}, and the aryl substituted NHT^{Mes} for which 0.5 equiv. are required to generate stable, well dispersed Pt NPs (NP mean-size 1.3(0.2)–1.5(0.2) nm, Fig. 3), with smaller amounts leading to platinum black. Increasing the length of the alkylic chain such as in NHT^{C18} is beneficial, since the decomposition process can be successfully achieved either with 0.2 and 0.5 equiv. of this ligand.

Finally, the very bulky NHT^{IPr} is not able to stabilize the nanoparticles at any concentration of the ligand. As will be discussed below, it is likely that the bulkiness of this ligand precludes an efficient coordination to the metal surface making this capping ligand inefficient towards stabilization of the metal nanoparticles.

These Pt colloids are rather soluble in organic solvents such as THF and benzene, allowing recording their ^1H NMR spectra. As expected from previous results on gold-NHT NPs,[13] the very broad signals showed in these spectra are consistent with the presence of platinum nanoparticles stabilized with organic ligands (see ESI, Fig. S2, S5, S8, S11, S14†).[19] The broadening of the signals is even more important when the proton atoms are closer to the surface of the metal nanoparticle, to the point that, in some cases, the signals can be lost in the base line. This seem to be the case for most of the colloids, for which no signals due to the back-bone of the imidazolyl fragment or the N–CH_2 are clearly discernible in their proton NMR spectra. This is indicating that such fragments are likely in very close proximity to the surface of the metal nanoparticle (see below).

High Resolution Transmission Electron Microscopy (HR-TEM) provides evidence for the crystallinity of the platinum NPs, with interplanar distances characteristic of (111) and (002) planes in the face-centered cubic structure (Fig. 4(a)–(d)). The EDX spectra recorded across various NPs of sample

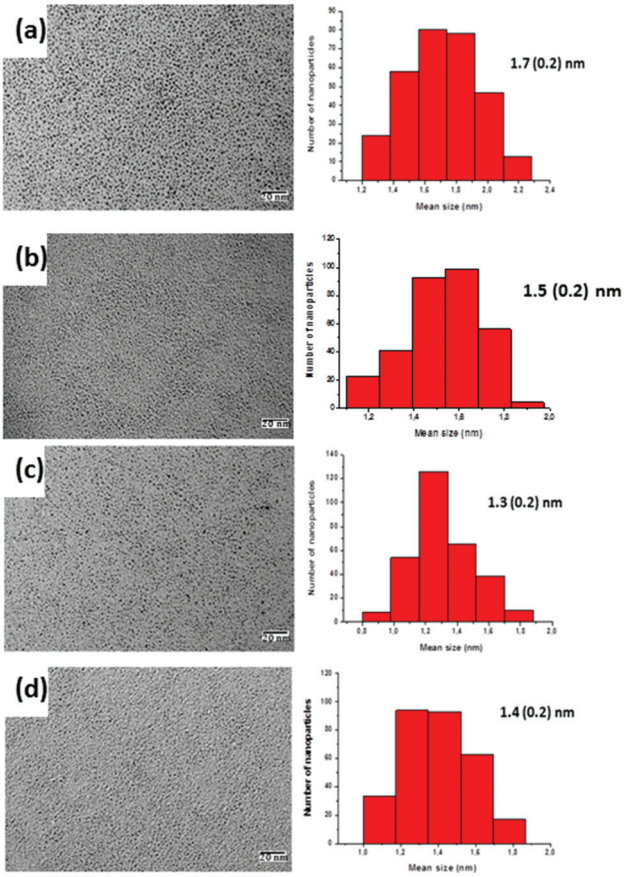

Fig. 3 TEM images and size distribution of platinum NPs: (a) PtNP-NHT^{C6},(b) PtNP- NHT^{C14},(c) PtNP-NHT^{Mes} and (d) PtNP-NHT^{C18}.

$PtNHT^{C6}$ using the scanning TEM (STEM) mode shows unequivocally three peaks at 2.1, 9.4 and 11.1 keV characteristic of platinum (besides the corresponding peaks of copper, carbon and Si arising from the grid and the specimen holder) (see Fig. 4(e)). The metal content was analyzed by Inductive Coupled Plasma (ICP) showing and array of values going from 31.65% (NHT^{C18}) to 68.66% (NHT^{Mes}) fitting very well with the values obtained for the content of organic material by TGA (see ESI† for details).

X-ray Photoelectron Spectroscopy (XPS) provided evidence for the coordination of the NHT to the surface of the platinum nanoparticle. In all the cases, the intensities (signal areas) of the signals in the spectra have been normalized by the relative intensity of the N 1s peak. The spectral regions of the Pt 4f, N 1s and S 2p peaks are depicted in Fig. 5.

The N 1s spectra for the four samples consist of a single, very symmetrical and narrow signal (fwhm = 1.7–1.9 eV) which indicates that a single chemical nitrogenated species are present in all the cases. The Pt 4f photoemission signal is a doublet, consisting of two energetic levels, Pt $4f_{7/2}$ and Pt $4f_{5/2}$, which are separated by 3.34 eV by electron spin–orbit interactions, with an intensity ratio of 0.75. For all the samples, the binding energy of the main peak, Pt $4f_{7/2}$, is in the range

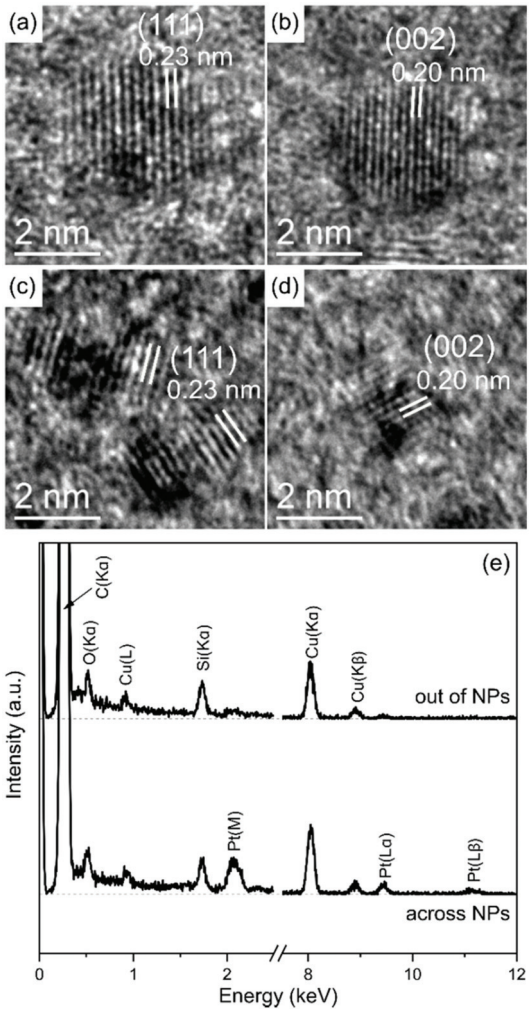

Fig. 4 HR-TEM images of platinum NPs: (a) and (b) PtNP-NHT^{Mes}, (c) and (d) PtNP-NHT^{C6}. (e) EDX spectra recorded across various NPs and across the support only (for reference).

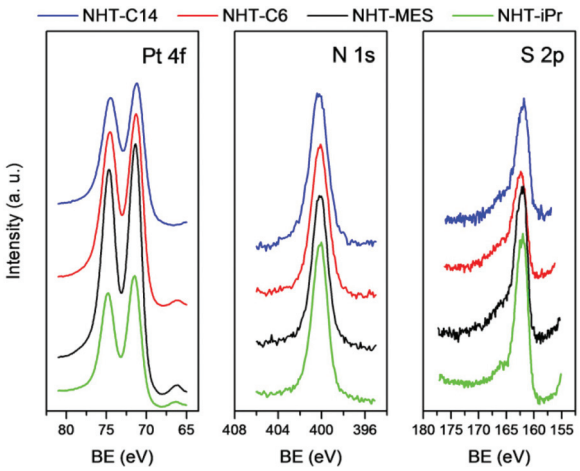

Fig. 5 Detailed X-ray photoelectron spectral regions for the main signals of the present elements in the four studied samples: Pt 4f, N 1s and S 2p.

71.3–70.9 eV, which are close to the binding energy of bulky metallic platinum (71.2 eV), and far away from the binding energy for Pt(II) or Pt(IV) compounds (in the range 73.6–76.3 eV).[20] In this sense, it must be noted that the electronic structure of nanometric particles can be strongly affected by their particle size and by the interaction with the environment. In particular, the Pt $4f_{7/2}$ binding energy for nanometric Pt particles increases when the particle size decreases when supported on "inert" substrates (for instance, up to 0.75 eV when supported on graphite).[21] Consequently, it can be assumed that platinum is present in metallic state for all the samples, while the small differences in their binding energy (≤0.46 eV) values could be caused by differences in the mean particle sizes or by interaction with the particular organic ligand. In the S 2p spectral region, an asymmetric signal is always found, consisting of a main peak at ~162.2 ± 0.2 eV with a long tail at the high binding energy side. The intensity, width and shape of this tail slightly differing among the samples (see discussion below).

The relative intensities of the signals provide us with additional pieces of information concerning the surface composition of the samples (Table 1). Importantly, the intensities (N/S atomic ratios) of the global S 2p spectra are quite similar for all samples.

A remarkable feature is that the N/S ratios are close to 2, consistent with the composition of the NHT ligands. Additionally, the relative values of the Pt/N ratios range from 1.02 to 1.99. These differences might be related to two factors: the adsorption of the organic molecule and the mean size of the platinum nanoparticles. With respect to the former, higher coverage degree of the surface and higher packing density of the adsorbate molecules, lead to lower Pt/N ratio. Concerning the particle size, for Pt particles with diameters lower than 3 nm, (which is the Pt 4f photoelectrons analysis depth),[22] the lower the mean size, the lower the Pt/N ratio (the Pt/N ratio will not be affected for particles diameters larger than 3 nm). Consequently, a lower Pt/N ratio could indicate a higher surface coverage of the Pt particles by the adsorbate or a smaller Pt particle diameter. However, since the mean sizes of the Pt nanoparticles, as determined by TEM, is in a very close range for all the studied samples, between 1.3 and 1.7 nm, it is reasonable to assume that the Pt/N atomic ratio is mainly determined by the adsorption coverage. Therefore, the Pt-NHT^{iPr} are highly covered by the ligand (Pt/N ratio = 1.02) whereas Pt-NHT^{Mes} are less covered, in agreement with the higher steric hindrance exerted by the mesityl groups in com-

Table 1 Quantitative analysis of the surface composition of the platinum colloids Pt-NHT^{iPr}, PNP-NHT^{Mes} PtNP-NHT^{C6} and PtNP-NHT^{C14}

	Pt_{4f} %At	N %At	S %At	N/S ratio	Pt/S ratio	Pt/N ratio
PtNP-NHT^{iPr}	6.55	6.41	3.43	1.87	1.91	1.02
PtNP-NHT^{Mes}	9.39	4.73	2.55	1.85	3.68	1.99
PtNP-NHT^{C6}	7.82	4.94	2.50	1.98	3.13	1.58
PtN-PNHT^{C14}	3.80	3.20	1.58	2.03	2.41	1.19

parison to the iso-propyl fragments. Nevertheless, the case for platinum nanoparticles PtNP-NHT^{C6} and PtNP-NHT^{C14} might be, in principle, counterintuitive. The longer length of the C14 side-chains should give rise to a more sterically hindered environment compared to the C6 alkyl chains. However, the Pt/N ratio observed (Table 1) suggest that the platinum nanoparticles have a higher content of NHT^{C14} ligands than the NHT^{C6}. It is not entirely understood the reasons underlying to this effect, but one possible explanation could be that the NHT^{C14} ligands are more packed around the surface as a consequence of lateral packing interactions of the alkyl chains, whereas the alkyl arms in NHT^{C6} are less ordered, spreading randomly, leading to a less covered surface.[23] In fact, according to theoretical calculations the interaction of two C14 chains is favored by *ca.* 5 kcal mol^{-1} (ΔE_{bind} = −3.3 *vs.* −8.1 kcal mol^{-1} for C6/C6 and C14/C14, respectively), supporting a preference for a more ordered structure.

The S 2p signals have been deconvoluted and fitted with three components (three doublets as shown in Fig. 6; see Experimental section for details). The energy position and the width of the main component is well defined for the four samples; the peak S 2p$_{3/2}$ is located at 161.8 ± 0.3 eV and its width is relatively low (fwhm = 1.9 ± 0.1 eV). However, the energy positions and widths of the second and third component are poorly defined due to instrumental noise: the peak S 2p$_{3/2}$ is located at 164.3 ± 0.5 eV and at 166.9 ± 0.5 eV for the second and third component, respectively, while their widths are around 20% wider (fwhm = 2.25 ± 0.15 eV) than that of the main component. Nonetheless, the proportions of the three components vary slightly from one sample to another. The minor component, with a proportion around 10% (with a high binding energy), is very likely related to some that oxidized sulfur species (sulphates, sulphites, ...), and it is a regular by-product in the study of adsorbed thiols on metal surfaces. It is worth comparing energy positions of free and coordinated thiones to that observed in the platinum nanoparticles reported herein. The S 2p signal from a free thiourea is located at ~162.4 ± 0.1 eV, while coordination to metal cations (such as Co(II), Ni(II), Cu(I), Re(IV)) through its sulfur atom leads to small positive S 2p chemical shifts (between +0.3 and +0.6 eV).[24] On the contrary, small negative chemical shifts can be expected for coordination of thiourea molecules to metal particles as previously reported on thiourea absorbed on polycrystalline platinum.[25] Consequently, the main component in the S 2p spectra observed for PtNPs-NHT is due to chemisorbed molecules to platinum atoms.

Theoretical calculations: DFT and DPD

In order to understand the role of NHT on the stabilization of PtNPs, theoretical calculations have been carried out using two approaches. Firstly, DFT calculations have been applied at the CAM-B3LYP-D3(BJ)/LanL2DZ level of theory to study the feasible coordination modes of different NHTs to PtNPs. In this context, the analysis of molecular electrostatic potential (MEP) surface of Pt_{10} subnanocluster reveals positive (+26 kcal mol^{-1}) and negative (−12 kcal mol^{-1}) regions on the surface highlighting the donor–acceptor ability of Pt nanoparticles thus enabling interactions with different moieties (Fig. 7). Expectedly, the most negative electrostatic potential is found for the thione (*ca.* −30 kcal mol^{-1}) moiety whereas the positive electrostatic potential (*ca.* +11 kcal mol^{-1}) is located in the C=C bond region. Therefore, both functional groups should have the capability to interact favourably with the PtNP surface. In fact, Pt-NHT^{iPr} and Pt-NHT^{C5} (as a model for a lineal alkylic NHT) exhibit large adsorption energies (ΔE_{ads} of −132.5 and −130.2 kcal mol^{-1}, respectively) showing thione (R_{S-Pt} = 2.42 Å) and C=C (R_{C-Pt} = 2.12 Å) groups chemisorbed onto the surface (Fig. 7). Even though the complexation of NHT^{Mes} and NHT^{iPr} are also equally favoured due to the presence of several Pt···H–C and Pt···π non-covalent interactions,[26] a different geometrical situation arises. NHT^{Mes} stabilizes Pt nanoparticles through chemisorption of the thione moiety whereas the C=C bond of the imidazolyl fragment is pointing outward far away from the Pt_{10} cluster. However, we roughly estimate a weaker coordination based on the directionality of Pt–S bond ($\varphi_{C=S-Pt}$ = 116° *vs.* 96° in NHT^{C5}). This situation

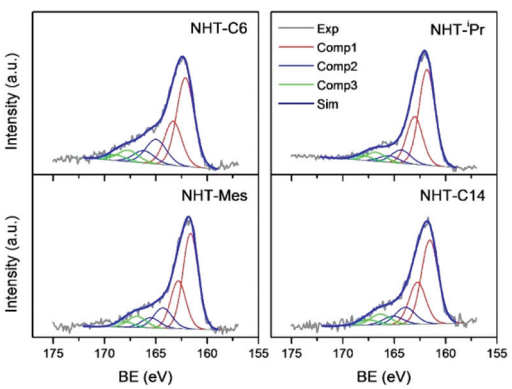

Fig. 6 Experimental and fitted S 2p X-ray photoelectron spectral region for the four studied samples PtNp-BHT^{C6}, PtNP-NHT^{iPr}, PtNP-NHT^{Mes} and PtNP-NHT^{C14}.

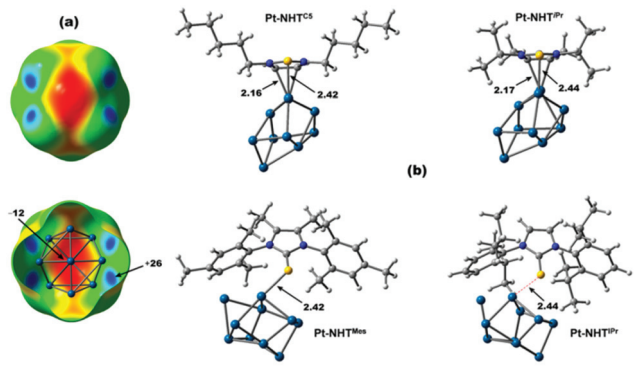

Fig. 7 (a) MEP of Pt nanoparticles plotted onto the 0.001 a.u. isodensity surface; (b) optimized structures for the interaction between Pt_{10} cluster and different NHT ligands at CAM-B3LYP-D3(BJ)/LanL2DZ level. Energies are given in kcal mol^{-1} and distances in Å.

ends up with loss of complexation observed for NHT^{iPr} (R_{S-Pt} = 2.44 Å, $\varphi_{C=S-Pt}$ = 117°) in agreement with experimental results about the stabilization of Pt nanoparticles with this NHT. At this point, we have used Dissipative Particles Dynamics (DPD) simulations as second approach to get further insight about the stabilization of Pt nanoparticles in THF by means of NHT ligands. Since we have correlated soft-repulsive parameters with DFT-based binding energies to build our coarse grained model (Fig. S18, ESI†),[27] this second approach is an efficient way to transfer the atomistic features to mesoscopic simulations. In fact, this kind of calculations encompasses different phenomena such as cooperativity and competitiveness between ligands as well as aggregation and stability over the time (temperature fixed at 23.5 °C) in a periodic environment.

Regarding the model, we have considered the stabilization of one Pt nanoparticle (formed by 100 beads) and lineal NHT^{C14} (50 molecules, 12 beads each one). In addition, Pt nanoparticle has a computed diameter of 1.6 nm in the range of experimental findings. After the simulation time (900 ns), PtNP is surrounded by *ca.* 20 NHT molecules (Fig. 8a). Radial distribution function (RDF) analysis reveals that both S and N/C=C moieties are located on the Pt surface although there is a subtle but clear preference for S beads, and therefore, thione groups. Nevertheless, the calculated distance from m_{PtNP} is around 0.2 nm, in agreement with R_{S-Pt} (and R_{C-Pt}) distance aforementioned in DFT calculations. An analogous simulation has been carried out to study the stabilization of one PtNP by hindered NHT^{Mes} (50 molecules, 10 beads each one). Interestingly, this system is stabilized much earlier than NHT^{C14} along the simulation time (125 *vs.* 450 ns, respectively). Despite being stabilized faster, the nanoparticle surface is covered by only 10% of NHT^{Mes} molecules (Fig. 8b). In this case, the outcomes of the analysis of RD functions provide differences between distances of S and N/C=C beads. In fact, the S beads are on the Pt NP surface while beads for mesityl groups are further away. In addition, the calculated distances of N/C=C beads from m_{PtNP} is even further away (around 1.07 nm; 0.27 nm from the surface) as expected for hindered NHT^{Mes} molecules.

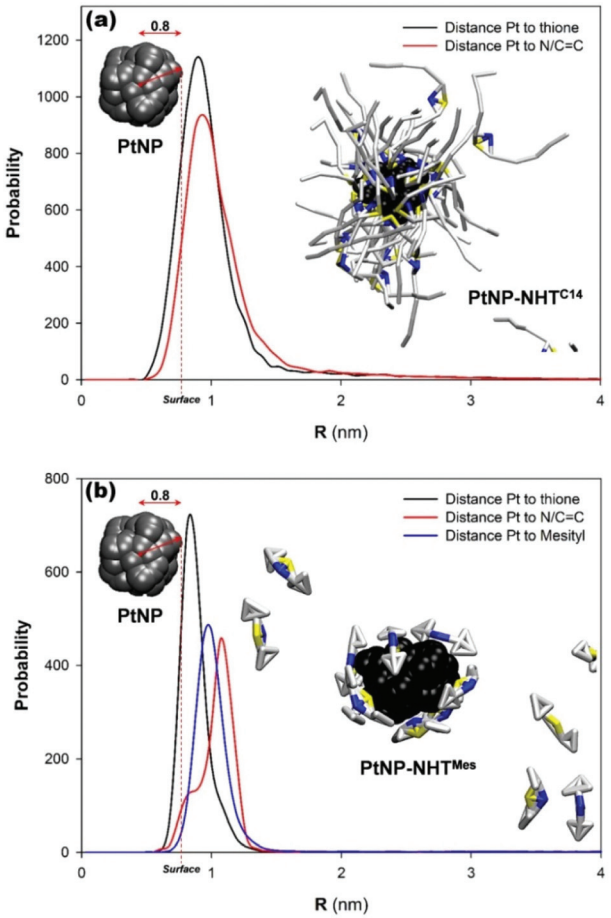

Fig. 8 (a) Radial distribution function for the distance between the center of mass and different functional groups of NHT^{C14}. Results from the simulations of one stabilized PtNP at 900 ns is also shown; (b) radial distribution function for the distance between the center of mass and different functional groups of NHT^{Mes} and final snapshot of the stabilization of one PtNP taken at 900 ns. Color codes: Pt in black, carbon in gray, sulfur in yellow, and the C=C/N beads in blue; THF beads have been removed for clarity.

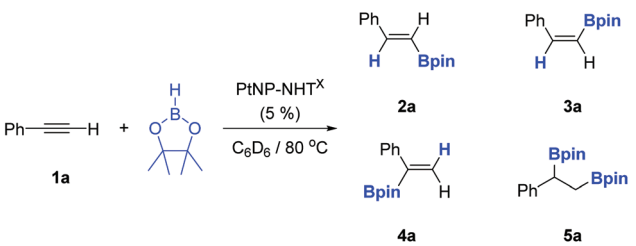

Scheme 2 Hydroboration of phenylacetylene catalyzed by different PtNp-NHT^{X} colloids.

Catalytic activity in hydroboration of alkynes

With the well-defined Pt nanoparticles in hand, we have tested their catalytic activity in the hydroboration of alkynes. First, we have used as a model reaction the hydroboration of phenylacetylene with a slight excess of pinacolborane,[28] using 5% of the PtNP colloid in benzene-d_6 at 80 °C (Scheme 2). The platinum colloids PtNP-NHT^{iPr}, PtNP-NHT^{Mes}, PtNP-NHT^{C6}, PtNP-NHT^{C14} and PtNP-NHT^{C18} have been evaluated in the process, and the results are collected in Table 2.

In all cases, both the mono- and di-borylated species **2a–5a** have been detected in variable amounts. However, the best system in terms of conversion, selectivity and time appeared to be the colloid PtNP-NHT^{Mes}, for which full conversion is achieved in only 4 h with an excellent selectivity towards the monoborylated, anti-Markovnikov *trans*-isomer **2a** (Table 2, entry 2). On the other hand colloids, PtNP-NHT^{iPr}, PtNP-NHT^{C6} and PtNP-NHT^{C14} exhibited a rather similar behaviour, but conversions below 45% are observed after 15–20 h (Table 2, entries 1, 3 and 4). The platinum nanoparticles, PtNP-NHT^{C18} did not show any catalytic activity. A

Table 2 Hydroboration of phenylacetylene catalyzed by different PtNP-NHT[a]

Entry	Catalyst	Time (h)	Conversion (%)	Selectivity (**2a** : **3a** : **4a** : **5a**)
1	PtNP-NHT^{iPr}	15	20	50 : 10 : 20 : 0[b]
2	PtNP-NHT^{Mes}	4	>99	79 : 6 : 5 : 5[c]
3	PtNP-NHT^{C6}	19	34	72 : 2 : 11 : <1[d]
4	PtNP-NHT^{C14}	20	44	66 : 3 : 10 : 7[e]
5	PtNP-NHT^{C18}	20	<5%	–[c]

[a] Reaction conditions: 0.35 mmol of phenylacetylene (1 M in C_6D_6), 0.36 mmol of HBpin, 5% PtNP-NHT^{X}, 80 °C. [b] 20% of styrene is formed. [c] 5% of styrene is formed. [d] 15% of styrene is formed. [e] 14% of styrene is formed.

possible explanation for the different performance of the alkyl-substituted NHT colloids compared to the very active PtNP-NHT^{Mes} might be related to a different coordination of the NHT to the surface of the platinum nanoparticle. As described above, the N-heterocyclic thiones substituted with alkyl chains seems to bind the surface using both the sulfur atom and the C=C double bond, with a flat disposition of the heterocyclic ring towards the metal surface. However, the approach of the C=C double bond of the mesityl derivative NHT^{Mes} is hampered by the aromatic rings, leading to coordination of the NHT exclusively through the S atom. This bonding situation might have two possible effects; first, the metal surface is more exposed to the incoming substrates, and second the NHT ligand is less effectively anchored to the surface facilitating its detachment to undergo exchange with the substrates. These effects together with the fact that, according to XPS (see above), the colloid PtNP-NHT^{Mes} is less covered by ligands, are likely responsible for the enhanced catalytic activity of PtNP-NHT^{Mes} in comparison to the other nanoparticles due to the presence of more active sites.

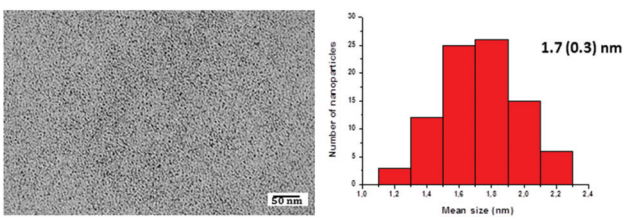

Fig. 9 TEM images of the colloid PtNP-NHTMes after a catalytic reaction.

At this point it's worth mentioning that the morphology and size of the metal nanoparticles are retained after the catalytic process, as shown in the TEM image of Fig. 9 obtained from the content of the crude reaction mixture solutions after hydroboration of phenylacetylene with pinacolborane. This analysis revealed the presence of individual nanoparticles with a similar mean size than the starting material (1.7(0.3) nm; Fig. 9).

Once established the most efficient catalytic system, several reaction conditions were tested. The solvent, temperature and catalyst loadings were modified and the results are summarized in Table 3. The catalyst loading has an influence on the rate of the reaction but only marginally on the selectivity. On the other hand, lower catalyst loadings (1 and 2%, entries 5–8) lead to good selectivities towards the monoborylated product **2a**, but slightly longer times are required to achieve full conversion. In this sense an increase of the reaction temperature to 80 °C is clearly beneficial, reducing about 2 h the reaction time (entries 5–7 *vs.* 6–8), and increasing slightly the monoborylated species **2a** to levels even higher than those values found using 5% of catalyst loadings at the same temperature (see Table 2, entry 2). As will be discussed below, the better selectivity observed under lower catalyst loadings is likely related to changes in the active catalyst species during the course of the reaction.

The effect of the solvent has been also explored with tetrahydrofurane-d_8 or acetonitrile-d_3 (Table 3, entries 9 and 10).

However, the results were in all cases poorer in terms of activity, selectivity or rate. Therefore, coordinating solvents such as THF or acetonitrile, inhibit to some extent the catalytic process according to their ligand binding properties.

The scope of the reaction has been explored by using, initially, terminal and internal aromatic alkynes bearing electron-donor and withdrawing groups under the optimized reaction conditions (1% cat., 80 °C, benzene-d_6). The conversion and selectivity has been determined by means of NMR and/or

Table 3 Optimization of the reaction conditions using phenylacetylene, pinacolborane and colloid PtNP-NHT^{Mes} as catalyst

Entry	Catalyst loading (%)	Solv.	*T* (°C)	Time (h)	Conv. (%)	Selectivity (**2a** : **3a** : **4a** : **5a**)[a]
1	5.0	C_6D_6	60	12	>99	79 : 2 : 2 : 16
2	5.0	C_6D_6	70	4	>99	76 : 3 : 4 : 11
3	3.0	C_6D_6	60	12	>99	84 : 2 : 2 : 10
4	3.0	C_6D_6	70	4	>99	87 : 2 : 2 : 8
5	2.0	C_6D_6	70	6	>99	86 : 2 : 2 : 8
6	2.0	C_6D_6	80	4	>99	88 : 3 : 1 : 6
7	1.0	C_6D_6	70	8	>99	87 : 1 : 1 : 10
8	1.0	C_6D_6	80	6.5	>99	88 : 2 : 1 : 7
9	1.0	THF d_8	80	15	79	89 : 2 : 0 : 6
10	1.0	CD_3CN	80	24	>99	83 : <1 : <1 : 16

[a] In all cases minor amounts of styrene (less than 2%) was observed.

GC-MS. The monoborylated products (*E* isomers in the case of terminal alkynes and *Z* for internal) have been obtained in all cases as the major product in reaction times going from 4 to 60 h (Table 4). The presence of electron–donor or withdrawing groups has an effect on the reaction rate but not significantly on the selectivity (small amounts of diborylated species were detected). In all cases the major product is the one arising from a *syn* addition of the borane in an *anti*-Markovnikov manner. The yield of products formed through the *anti*- or the Markovnikov additions is, typically, below 7%.

The reaction using electron donor groups in the *para* position of the aromatic ring took place considerably faster than with electron-withdrawing fragments (Table 4, alkynes **1b,c** *vs.* **1d,e**). Nevertheless, the effect of groups in the *ortho* position was very diverse and difficult to rationalize. For example, the presence of F and CF_3 groups in the *ortho* position (Table 4, alkynes **1h,i**) decreases and increases the rate of the reaction, respectively, in comparison with their *para* substituted counterparts (alkynes **1d,e**). With respect to the selectivity of the process, the *ortho* substituents slightly favour the amount of the monoborylated products. The borylation process has been extended to both aromatic and aliphatic internal alkynes. Besides obtaining full conversion in all cases, the reactions were considerably faster than those of the terminal alkynes, taking place in as short as 1 h (Table 4, alkynes **1j–l**). Although excellent selectivities are obtained for diphenylacetylene and 3-hexyne, the asymmetrical 1-phenyl-1-propyne generates mixtures of isomers **2l** and **2l′** in a 1 : 3.7 ratio together with a poorer selectivity with respect to the diborylated isomer (Scheme 3).

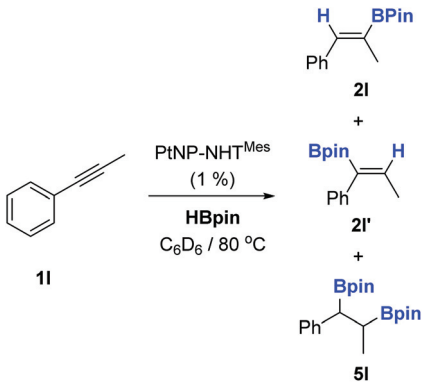

Scheme 3 Hydroboration of 1-phenyl-1-propyne catalyzed by PtNP-NHT^{Mes}.

Table 4 Hydroboration under optimized conditions of different alkynes catalyzed by PtNP-NHT^{Mes} [a]

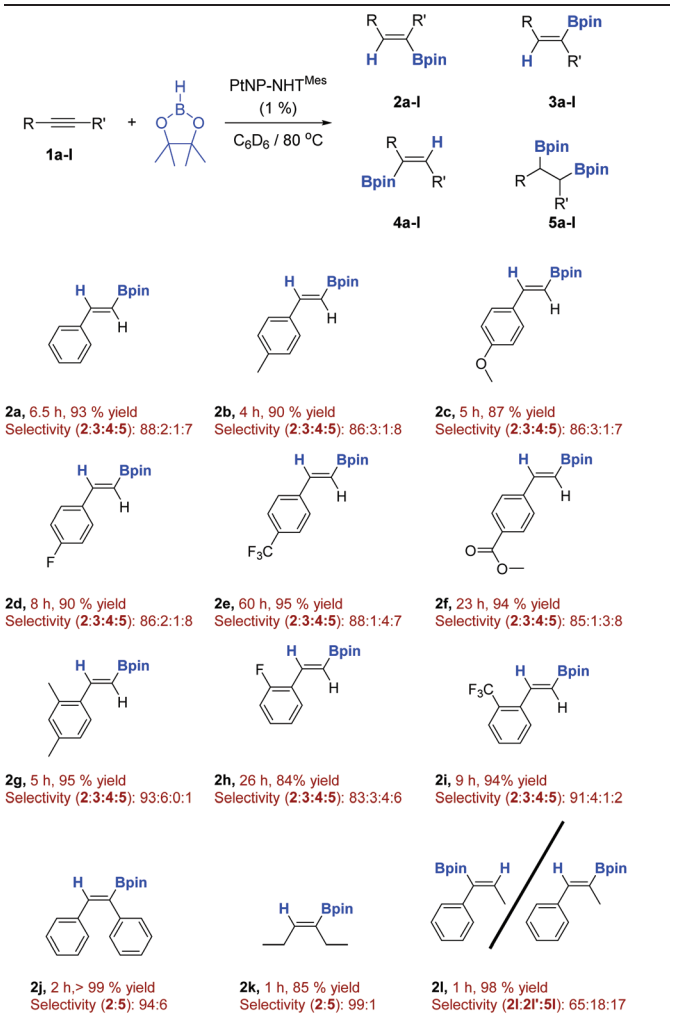

[a] Yields are given for the inseparable mixture of compounds **2–5**.

As for aromatic systems, terminal aliphatic alkynes can be efficiently hydroborated, but as inferred from the data shown in Table 5, the selectivity of the process is slightly poorer, in which the diborylated species are produced in amounts ranging from 4 to 13% of the total amount. In fact, at variance to the results obtained for aromatic alkynes, when the reaction is carried out with an excess (3 equiv.) of pinacolborane, full conversion to the diborylated derivatives is produced, generated as mixtures of the 1,2 and 1,1dihydroboration reaction (Scheme 4 and Table 6). The ratio of these isomers depends strongly on the bulkiness of the alkyl moiety at the 3 position of the alkyne. Thus, the less hindered systems (Table 6, alkynes **1p–r**) lead to an approximately 2 : 1 ratio in favour to the 1,1 disubstituted alkylborane, whereas the presence of a bulkier group such as cyclopropyl, cyclohexyl or iso-propyl, increase the selectivity up to 100% (alkynes **1m–o**). Interestingly, under these reaction conditions (excess of borane) no 1,2-diborylated species is formed for the cyclopropylacetylene **1m**, in stark contrast with the reaction of this

Table 5 Hydroboration under optimized conditions of different terminal aliphatic alkynes catalyzed by PtNP-NHT^{Mes} [a]

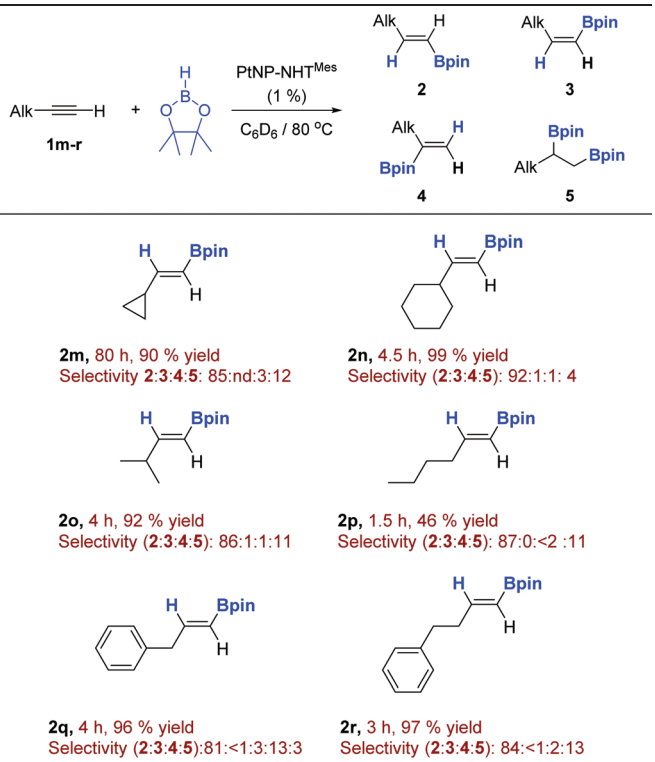

[a] Yields are given for the inseparable mixture of compounds **2–5**.

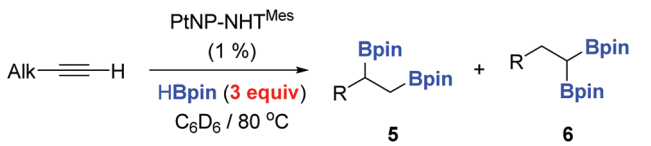

Scheme 4 Dihydroboration of terminal alkyl-alkynes with an excess of pinacolborane.

alkyne with 1.2 equiv. of borane, a reaction that produces small amounts of the 1,2-diborylated derivative **5m** with no signs of **6m** being detected. We do not have an explanation to this contradictory result, but a possible explanation might be found in a different active surface catalyst, when the reaction is carried out in the presence of an excess of pinacolborane, or in a different active catalyst that is only present at early stages of the reaction. This latter assumption might also explain the formation of small amounts of 1,2-diborylated species in the reaction of aromatic alkynes with pinacolborane that, as stated above, do not increase with either time or in the presence of an excess of the borane.

Although the hydroboration of alkynes leading to vinylboronates (monoborylation) has been previously studied using NHC-stabilized Pt nanoparticles,[10c] this is the first time that diborylation products have been obtained using platinum nanoparticles.

Table 6 Hydroboration of different terminal aliphatic alkynes catalyzed by PtNP-NHT^{Mes} using 3 equiv. of HBpin [a]

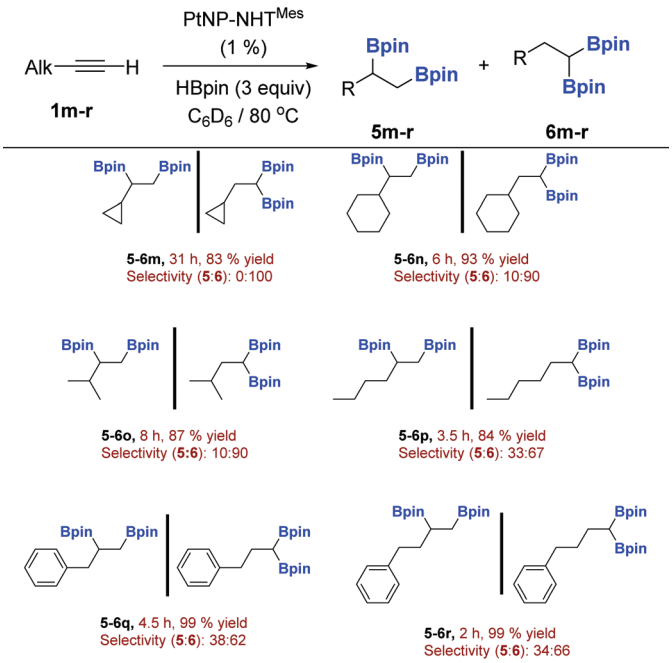

[a] Yields are given for the inseparable mixture of compounds **5** and **6**.

Conclusions

Readily available, air stable N-heterocyclic thiones (NHTs), are excellent ligands for the synthesis and stabilization of well-defined, small platinum nanoparticles. The surface coverage can be controlled through the modification of the steric environment on the nitrogen atoms of the NHT ligands. XPS clearly indicate that the NHT is bound to the metal through the sulphur atom but, in addition, according to DFT calculations, further stabilization through coordination of the C=C double bond of the imidazole moiety is present when relatively small substituents are present on the nitrogen atoms. Larger substituents, such as mesityl, disfavours this type of interaction, likely due to steric repulsions of the flanking mesityl groups with the metal surface. These metal nanoparticles are active in the catalytic hydroboration of terminal and internal alkynes and, interestingly, the most active one is PtNP-NHT^{Mes} containing the smallest amount of ligand per surface area and lacking the interaction of the C=C double bond with the metal surface. The metal nanoparticles PtNP-NHT^{Mes} showed an excellent performance in the hydroboration of alkynes in terms of selectivity (leading to the anti-Markonikov vinyl-boronate products) and activity when one equivalent of borane is used but, additionally, the vinyl-boronate products can be further hydroborated to the 1,1- and 1,2-diborylated alkanes when aliphatic alkynes are used as starting materials. The selectivity of this latter process can be directed towards the 1,1-diborylated species by increasing the steric environment of the alkyne at the 3 position.

Conflicts of interest

There are no conflicts to declare.

Acknowledgements

Financial support (FEDER contribution) from the MINECO (Projects CTQ2016-76267-P, CTQ2016-80814-R and CTQ2016-81797-REDC) and the Junta de Andalucía (Project FQM-2126) is gratefully acknowledged. R. C. F thanks Conselho Nacional de Desenvolvimento Científico e Tecnológico (CNPq-CsF) and Fundación Carolina for financial support. L. C. M. thanks the CAPES Foundation, Ministry of Education of Brazil (CAPES-CsF 13465-13-9) for a doctoral grant. B. L. acknowledges the "Talent Attraction Program" of the University of Cádiz for supporting his research (contract code E-11-2017-0117214). We acknowledge support of the publication fee by the CSIC Open Access Publication Support Initiative through its Unit of Information Resources for Research (URICI).

Notes and references

1 (*a*) C. Amiens, D. Ciuculescu-Pradines and K. Philippot, *Coord. Chem. Rev.*, 2016, **308**, 409–432; (*b*) M. Zahmakıran and S. Özkar, *Nanoscale*, 2011, **3**, 3462–3481; (*c*) *Metal NPs: Preparation, Characterization and Applications*, ed. D. L. Feldheim and A. F. Colby Jr, Marcel Dekker, New York, 2002; (*d*) *The chemistry of Nanomaterials; Synthesis, Properties and Applications*, ed. N. R. Rao, A. Müller and A. K. Cheetham, C. Wiley-VCH, Weinheim, 2004, vol. 1 and 2; (*e*) *Handbook of Nanoparticles*, ed. M. Aliofkhazraei, Springer, 2016.

2 (*a*) L. Wang, A. Holewinski and C. Wang, *ACS Catal.*, 2018, **8**, 9388–9398; (*b*) M. Shao, A. Peles and K. Shoemaker, *Nano Lett.*, 2011, **11**, 3714–3719.

3 (*a*) S. B. Vendelbo, C. F. Elkjær, H. Falsig, I. Puspitasari, P. Dona, L. Mele, B. Morana, B. J. Nelissen, R. van Rijn, J. F. Creemer, P. J. Kooyman and S. Helveg, *Nat. Mater.*, 2016, **13**, 884–890; (*b*) R. M. Arán-Ais, F. J. Vidal-Iglesias, M. J. S. Farias, J. Solla-Gullón, V. Montiel, E. Herrero and J. M. Feliua, *J. Electroanal. Chem.*, 2017, **793**, 126–136.

4 T. Galeandro-Diamant, M.-L. Zanota, R. Sayah, L. Veyre, C. Nikitine, C. de Bellefon, S. Marrot, V. Meille and C. Thieuleux, *Chem. Commun.*, 2015, **51**, 16194–16196.

5 (*a*) D. Astruc, *Nanoparticles and Catalysis*, Wiley-VCH, Weinheim, 2008; (*b*) *Nanoparticles and Catalysis*, ed. P. Serp and K. Philippot, Wiley-VCH, Weinheim, 2013.

6 (*a*) L. Bai, X. Wang, Q. Chen, Y. Ye, H. Zheng, J. Guo, Y. Yin and C. Gao, *Angew. Chem., Int. Ed.*, 2016, **55**, 15656–15661; (*b*) W. Zang, G. Li, L. Wangab and X. Zhangab, *Catal. Sci. Technol.*, 2015, **5**, 2532–2553; (*c*) Y. Dai, Y. Wang, B. Liu and Y. Yang, *Small*, 2015, **3**, 268–289; (*d*) F. Zaera, *ChemSusChem*, 2013, **6**, 1797–1820; (*e*) K. An and G. A. Somorjai, *ChemCatChem*, 2012, **4**, 1512–1524; (*f*) K. M. Bratlie, H. Lee, K. Komvopoulos, P. Yang and G. A. Somorjai, *Nano Lett.*, 2007, **7**, 3097–3101.

7 (*a*) S. Tricard, O. Said-Aizpuru, D. Bouzouita, S. Usmani, A. Gillet, M. Tassé, R. Poteau, G. Viau, P. Demont, J. Carreya and B. Chaudret, *Mater. Horiz.*, 2017, **4**, 487–492; (*b*) P. Wanda, E. Kratzer, U. Heiz, M. Cokoja and M. Tschurl, *Catal. Commun.*, 2017, **100**, 85–88; (*c*) K. A. San and Y.-S. Shon, *Nanomaterials*, 2018, **8**, 346; (*d*) K. A. San, V. Chen and Y.-S. Shon, *ACS Appl. Mater. Interfaces*, 2017, **9**, 9823–9832; (*e*) F. Raynal, A. Etcheberry, S. Cavaliere, V. Noël and H. Perez, *Appl. Surf. Sci.*, 2006, **252**, 2422–2431; (*f*) S. E. Eklund and D. E. Cliffel, *Langmuir*, 2004, **20**, 6012–6018; (*g*) J. Yang, J. Y. Lee, T. C. Deivaraj and H.-P. Too, *Langmuir*, 2003, **19**, 10361–10365; (*h*) F. Dassenoy, K. Philippot, T. O. Ely, C. Amiens, P. Lecante, E. Snoeck, A. Mosset, M.-J. Casanove and B. Chaudret, *New J. Chem.*, 1998, 703–711.

8 P. Wand, J. D. Bartl, U. Heiz, M. Tschurl and M. Cokoja, *J. Colloid Interface Sci.*, 2016, **478**, 72–80.

9 (*a*) I. Schrader, J. Warneke, J. Backenköhler and S. Kunz, *J. Am. Chem. Soc.*, 2015, **137**, 905–912; (*b*) E. Morsbach, M. Nesselberger, J. Warneke, P. Harz, M. Arenz, M. Bäumera and S. Kunz, *New J. Chem.*, 2015, **39**, 2557–2564; (*c*) J. H. Ryu, S. S. Han, D. H. Kim, G. Henkelman and H. M. Lee, *ACS Nano*, 2011, **5**, 8515–8522; (*d*) M. Cabié, S. Giorgio, C. R. Henry, M. R. Axet, K. Philippot and B. Chaudret, *J. Phys. Chem. C*, 2010, **114**, 2160–2163; (*e*) E. Ramirez, L. Eradès, K. Philippot, P. Lecante and B. Chaudret, *Adv. Funct. Mater.*, 2007, **17**, 2219–2228; (*f*) J. Yang, J. Y. Lee and H.-P. Too, *Anal. Chim. Acta*, 2006, **571**, 206–210; (*g*) J. Yang, T. C. Deivaraj, H.-P. Too and J. Y. Lee, *J. Phys. Chem. B*, 2004, **108**, 2181–2185.

10 (*a*) Y. Zeng, T. Zhang, M. R. Narouz, C. M. Crudden and P. H. McBreen, *Chem. Commun.*, 2018, **54**, 12527–12530; (*b*) J. M. Asensio, S. Tricard, Y. Coppel, R. Andrés, B. Chaudret and E. de Jesús, *Chem. – Eur. J.*, 2017, **23**, 13435–13444; (*c*) L. M. Martínez-Prieto, L. Rakers, A. M. López-Vinasco, I. Cano, Y. Coppel, K. Philippot, F. Glorius, B. Chaudret and P. W. N. M. van Leeuwen, *Chem. – Eur. J.*, 2017, **23**, 12779–12786; (*d*) E. A. Baquero, S. Tricard, J. C. Flores, E. de Jesús and B. Chaudret, *Angew. Chem., Int. Ed.*, 2014, **53**, 13220–13224; (*e*) P. Lara, A. Suárez, V. Collière, K. Philippot and B. Chaudret, *ChemCatChem*, 2014, **6**, 87–90.

11 L. M. Martínez-Prieto, I. Cano, A. Márquez, E. A. Baquero, S. Tricard, L. Cusinato, I. del Rosal, R. Poteau, Y. Coppel, K. Philippot, B. Chaudret, J. Cámpora and P. W. N. M. van Leeuwen, *Chem. Sci.*, 2017, **8**, 2931–2941.

12 P. Hu, L. Chen, X. Kang and S. Chen, *Acc. Chem. Res.*, 2016, **49**, 2251–2260.

13 L. C. Moraes, B. Lacroix, R. C. Figueiredo, P. Lara, J. Rojo and S. Conejero, *Dalton Trans.*, 2017, **46**, 8367–8371.

14 Y. Zhua and N. S. Hosmaneb, *Coord. Chem. Rev.*, 2015, **293–294**, 357–367.

15 Synthesis and Applications of Organoboron Compounds, in *Topics in Organometallic Chemistry*, ed. E. Fernández and A. Whiting, Springer, Heidelberg, 2015.

16 (*a*) H.-Y. Tsai, M. Madasu and M. H. Huang, *Chem. – Eur. J.*, 2019, **25**, 1300–1303; (*b*) S. Thoka, M. Madasu, C.-F. Hsia, S.-Y. Liu and M. H. Huang, *Chem. – Asian J.*, 2017, **12**, 2318–2322; (*c*) A. Khan, A. M. Asiri, S. A. Kosa, H. Garcia and A. Grirrane, *J. Catal.*, 2015, **329**, 401–412; J. Zhao, Z. Niu, H. Fu and Y. Li, *Chem. Commun.*, 2014, **50**, 2058–2060; (*d*) S. Rawat and B. Sreedhar, *Synlett*, 2014, **25**, 1132–1136.

17 (*a*) R. Nallagonda, K. Padala and A. Masarwa, *Org. Biomol. Chem.*, 2018, **16**, 1050–1064; (*b*) S. Lee, D. Li and J. Yun, *Chem. – Asian J.*, 2014, **9**, 2440–2443; (*c*) Z. Zuo and Z. Huang, *Org. Chem. Front.*, 2016, **3**, 434–438; (*d*) J. Takaya and N. Iwasawa, *ACS Catal.*, 2012, **2**, 1993–2006.

18 (*a*) P. Lara, K. Philippot and B. Chaudret, *ChemCatChem*, 2013, **5**, 28–45; (*b*) C. Amiens, B. Chaudret, D. Ciuculescu-Pradines, V. Collière, K. Fajerwerg, P. Fau, M. Kahn, A. Maisonnat, K. Soulanticac and K. Philippot, *New J. Chem.*, 2013, **37**, 3374–3401; (*c*) K. Philippppot and B. Chaudret, Organometallic Derived-I: Metals, Colloids and Nanoparticles, in *Comprehensive Organometallic Chemistry III*, ed. R. H. Crabtree and M. P. Mingos, Elsevier, Amsterdam, vol. 12, 2007.

19 L. E. Marbella and J. E. Millstone, *Chem. Mater.*, 2015, **27**, 2721–2739.

20 D. Briggs and M. P. Seah, *Practical Surface Analysis by Auger and X-ray Photoelectron Spectroscopy. Apendix 5*, Wiley, Chichester, 1983, p. 621.

21 M. G. Mason, *Phys. Rev. B*, 1983, **27**, 748–762.

22 S. Tanuma, C. J. Powell and D. R. Penn, *Surf. Interface Anal.*, 2011, **43**, 689–713.

23 (*a*) J. Kubackova, I. Izquierdo-Lorenzo, D. Jancura, P. Miskovskybcd and S. Sanchez-Cortes, *Phys. Chem. Chem. Phys.*, 2014, **16**, 11461–11470; (*b*) S. T. Marshall, M. O'Brien, B. Oetter, A. Corpuz, R. M. Richards, D. K. Schwartz and J. W. Medlin, *Nat. Mater.*, 2010, **9**, 853–858; (*c*) L. Guerrini, I. Izquierdo-Lorenzo, J. V. Garcia-Ramos, C. Domingo and S. Sanchez-Cortes, *Phys. Chem. Chem. Phys.*, 2009, **11**, 7363–7371.

24 V. Srinivasan and R. A. Walton, *Inorg. Chim. Acta*, 1977, **25**, L85–L86.

25 M. Quinet, F. Lallemand, L. Ricq, J. Y. Hihn and P. Delobelle, *Surf. Coat. Technol.*, 2010, **204**, 3108–3117.

26 J. Cordón, G. Jiménez-Osés, J. M. López-de-Luzuriaga and M. Monge, *Nat. Commun.*, 2017, **8**, 1657.

27 A. Franconetti, J. M. Carnerero, R. Prado-Gotor and F. Cabrera-Escribano, *Carbohydr. Polym.*, 2019, **207**, 806–814.

28 A slight excess of pinacolborane was necessary in all cases to achieve full conversion of the alkyne. Reactions carried out with only 1 equiv. of the borane resulted in incomplete conversions with similar selectivities for both the mono- and diborylated species.